Electronic Supplementary Information

Fast photocatalytic degradation of rhodamine B by indium-porphyrin based cationic MOF under visible light

Chang-Xun Dou,[ab] Xu-Ke Tian,[ab] Ying-Jun Chen,[b] Pei-Pei Yin,[b] Jia-hui Guo,[b] Xiao-Gang Yang,*[b] Yu-Ming Guo*[a] and Lu-Fang Ma[ab]

[a]School of Chemistry and Chemical Engineering, Henan Normal University, Xinxiang, 453007, P. R. China. E-mail: guoyuming@htu.edu.cn

[b]College of Chemistry and Chemical Engineering, Luoyang Normal University, Luoyang 471934, P. R. China. E-mail: yxg2233@126.com.

A. Experimental Section

1. Materials and general procedures.

All reagents were of analytical grade and obtained from commercial sources without further purification. Powder X-ray diffraction (PXRD) patterns were measured at room temperature using a Bruker D8-ADVANCE X-ray diffractometer with Cu *Kα* radiation (λ = 1.5418 Å). Intensity data were collected in a 2θ range of 5-50° with a step of 0.02° (2*θ*) and a counting time of 0.2 s/step. The operating power was 40 kV, 40 mA. Thermogravimetric analysis (TGA) experiments were performed under a nitrogen atmosphere at a heating rate of 10 ℃ minutes^{-1} using an SⅡEXSTAR6000 TG/DTG6300 thermal analyzer from ambient temperature to 800 ℃. The UV-vis absorption spectra were recorded on a Shimadzu UV-3600 plus UV-vis-NIR spectrophotometer in the wavelength range of 200−800 nm. The surface morphologies of MOF sample were characterized by a field emission scanning electron microscope (SEM, Zeiss Sigma 500) at 5 kV. The degradation rates of dye solutions were periodically scanned by a UV-visible spectrophotometer (UV-5500PC, METASH). X-ray photoelectron spectroscopy (XPS) measurements were performed with the Thermo Scientific K-AIpha and equipped with a non-monochromatized source (at 150 W). Room temperature PL spectra and time-resolved lifetime were conducted on an Edinburgh FLS1000 fluorescence spectrometer equipped with a xenon arc lamp (Xe900) and nanosecond flash-lamp (nF900).

Single-crystal X-ray diffraction data for complex **1** were collected using an Oxford Diffraction SuperNova area-detector diffractometer and mirror optics monochromated Mo Kα radiation (λ = 0.71073 Å) at normal temperature (293K). CrysAlisPro was used for the data collection, data reduction, and empirical absorption correction. The crystal structure was solved by direct methods, using SHELXS-2014 and lasted-squares refined with SHELXL-2014, and all other non-hydrogen atoms were refined with anisotropic thermal displacement parameters. The crystallographic data and selected bond lengths and angles for **1** were listed in Tables S2-S3. Crystallographic data for the structural analyses have been deposited with the Cambridge Crystallographic Data Center. CCDC number for **1** is 2269364.

This material can be obtained free of charge via http://www.ccdc.cam.ac.uk/conts/retrieving.html, or from the Cambridge Crystallographic Data Centre, 12 Union Road, Cambridge CB2 1EZ, UK; fax: (+44) 1223-336-033; or E-mail: deposit@ccdc.cam.ac.uk.

Photoelectrochemical activities were performed with a Chenhua CHI 660E electrochemical workstation in a standard three-electrode system using a 0.5 M sodium sulfate aqueous solution as an electrolyte. The platinum wire electrode was used as a counter electrode, a saturated calomel electrode (SCE) was used as the reference electrode, and a certain amount of **1** coated indium tin oxide (ITO) was used as the working electrode with a working area of 1.0 cm^2. The system was conducted in a quartz glass reactor of ca. 50 cm^3 and irradiated by a 300 W xenon lamp. The cyclic voltammetry (CV) curves were investigated with a voltage range from -0.6 to 0.6 V (vs. Ag/AgCl) and scan rate of 50 mV/s. Electrochemical impedance spectroscopy (EIS) measurements were recorded at the potential of 0 V potential in the frequency range of 100 kHz to 100 MHz, and transient photocurrent responses with the on-off cycle's illumination were tested in the three-electrode system at ambient pressure and room temperature.

The photocatalytic activities of the **1** were evaluated by the degradation of Rhodamine B (RhB), methyl orange (MO) and methylene blue (MB) under visible light irradiation provided by a 300 W xenon lamp with a 420 nm cut off filter at room temperature in a 35 mL quartz reactor. In a typical process, a certain amount of photocatalyst **1** (10 mg) was immersed in 30 mL RhB (20 mg/L), MO (20 mg/L) MB (10 mg/L) aqueous solution for reserve. Prior to irradiation, the suspension was magnetically stirred in the dark for 0.5 h to achieve the adsorption-desorption equilibrium. Then the mixture solution was exposed to a visible light source (λ > 420 nm, 450 nm and 500 nm, respectively), and at certain intervals, 3mL of the suspension was subjected to ultraviolet-visible spectrophotometer analysis. Changes in the maximum absorbance of RhB at 554 nm, MO at 464 nm, and MB at 664 nm were measured spectrophotometrically to determine the decrease in the concentration of the three organic dyes. After the test, the suspension was put back into the reactor to continue the photocatalytic experiment, and the test was repeated.

2. Synthesis of [In(TPyP)]·(NO_3) (1).

A mixture of $In(NO_3)_2$ (0.0665 mmol, 20 mg) and 5,10,15,20-tetrakis(4-pyridyl)-21H,23H-porphyrin (TPyP, 0.0081 mmol, 5 mg) was dissolved in 6 mL N,N-dimethylformamide (DMF) solution containing 0.15 mL concentrated HNO_3. Then the mixture was sealed in a Teflon-lined stainless steel vessel reactor, which was heated to 120 °C for 48 hours before being naturally cooled to ambient temperature. Dark purple crystals were filtered, dried, and obtained in a natural environment. Elemental analysis calcd (%) for **1** $C_{40}H_{24}InN_9O_3$ (793.50): C 60.55, H 3.05, N 15.89. found: C 60.18, H 2.91, N 15.25.

B. Supporting Figures

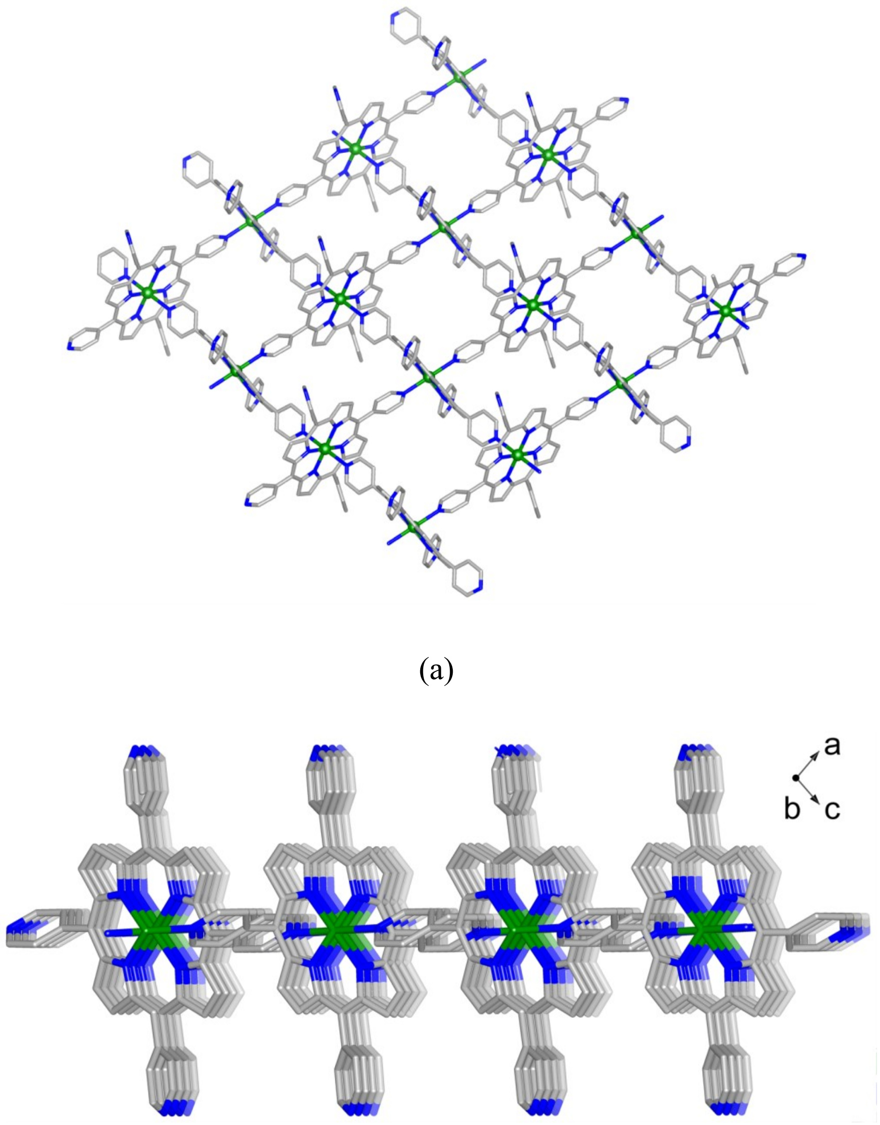

(a)

(b)

Figure S1. Top (a) and side (b) view of the 2D layer of **1**.

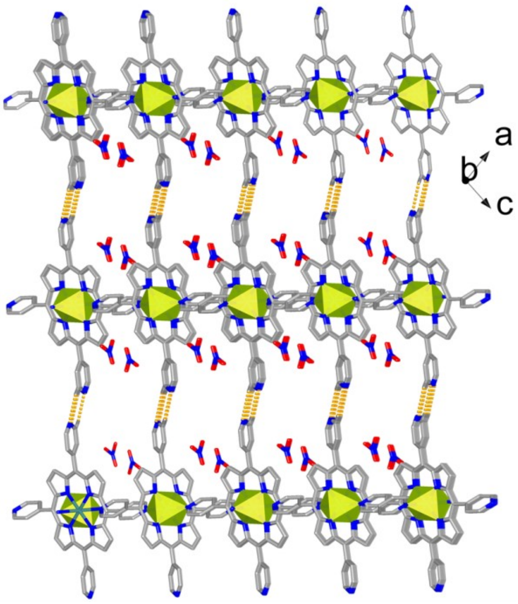

Figure S2. View of the 3D supramolecular network with the NO_3^- ions loading in the porous.

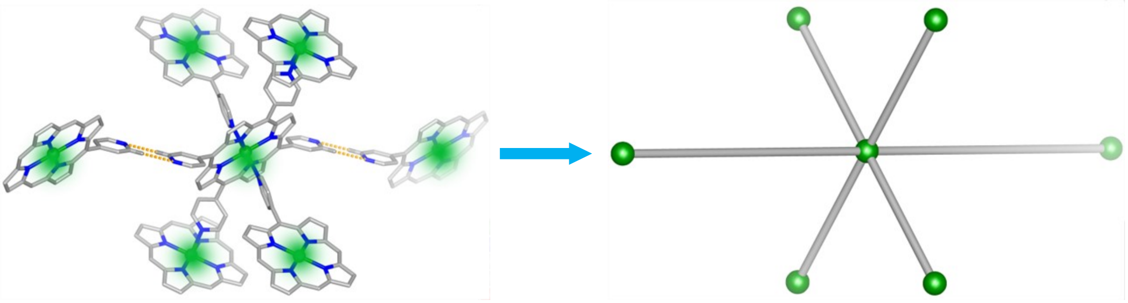

Figure S3. View of the 6-connected metalized TPyP node.

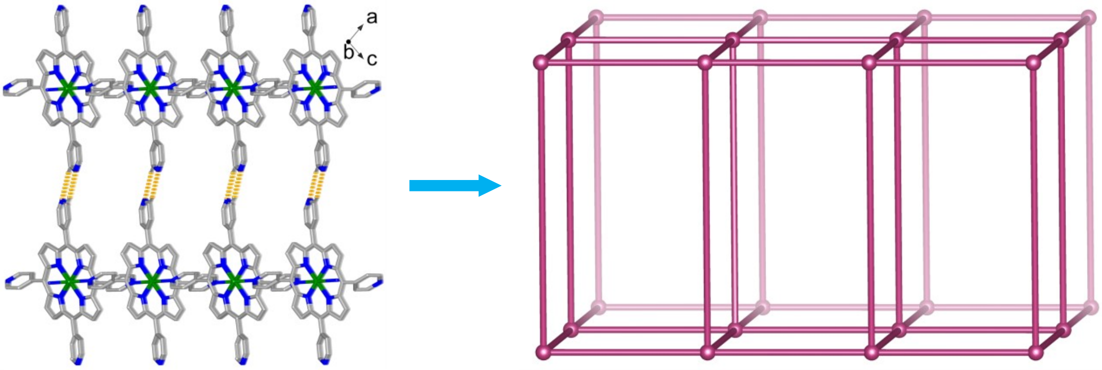

Figure S4. View of the 6-connected pcu network simplified from the 3D supramolecular network of **1**.

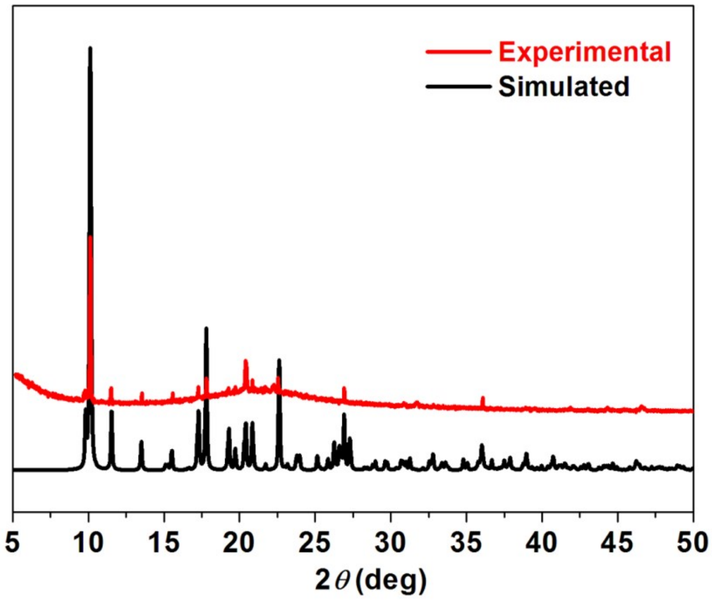

Figure S5. PXRD pattern of **1**.

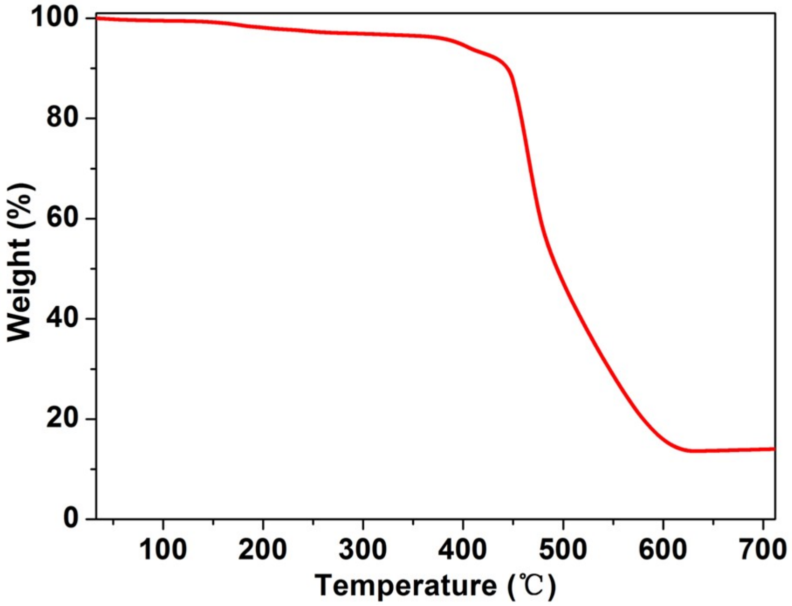

Figure S6. Thermogravimetric curve of **1**.

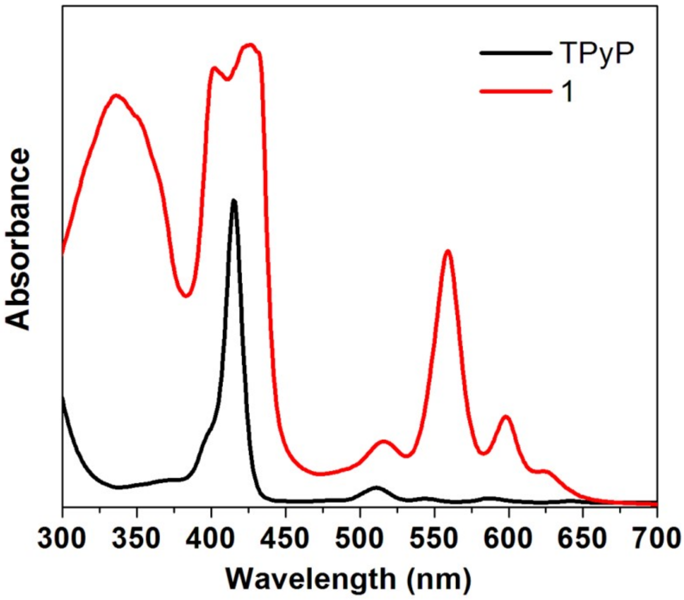

Figure S7. UV-vis spectra of complex **1** (red) and TPyP (black) in DMF (ca. 1 × 10^{-5} mol·L^{-1}).

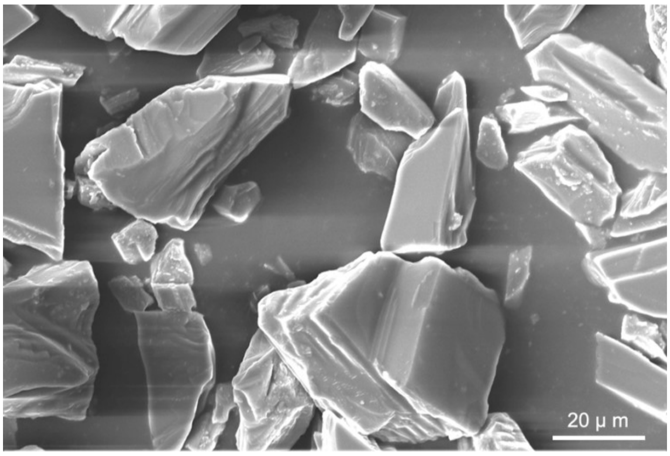

Figure S8. Scanning electron microscopy (SEM) image of the as-synthesized complex **1**.

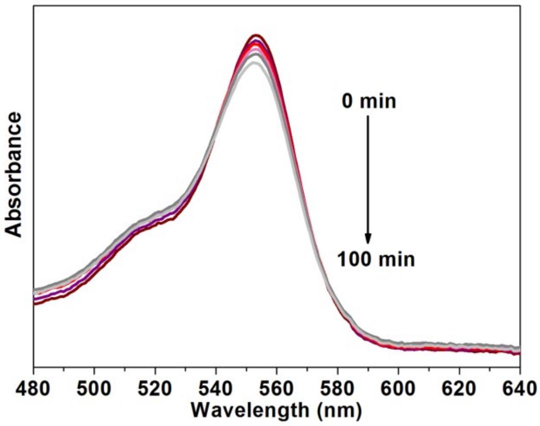

(a)

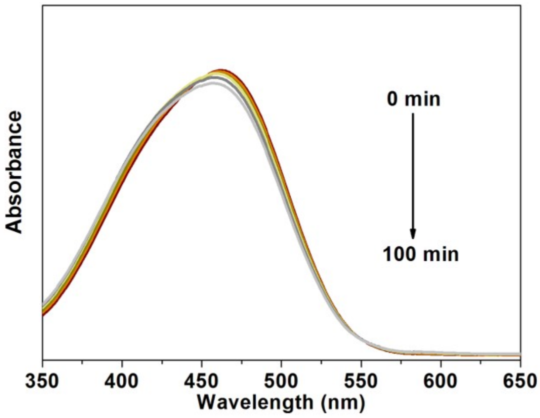

(b)

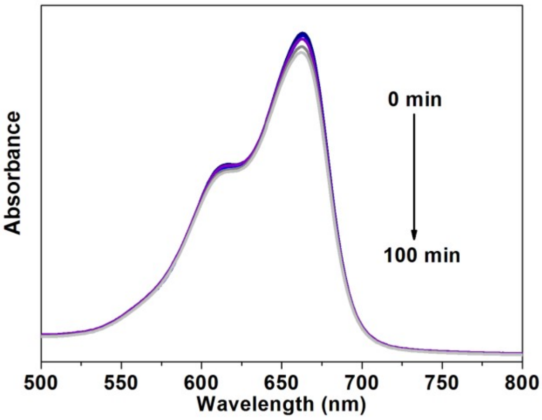

(c)

Figure S9. Self-degradation of RhB (a), MO (b) and MB (c) aqueous solution irradiated under visible light irradiation (λ > 420 nm).

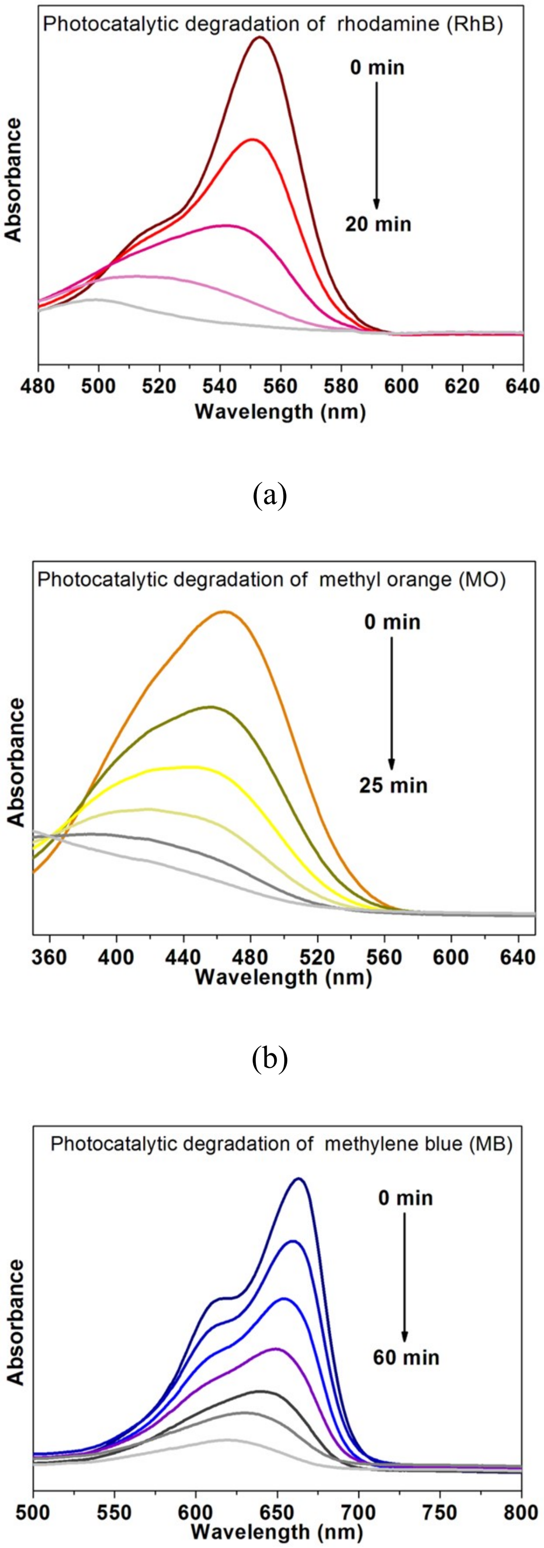

(a)

(b)

(c)

Figure S10. Degradation diagram of RhB (a), MO (b) and MB (c) with presence of the powder of complex **1** (10 mg) under visible light irradiation ($\lambda > 420$ nm).

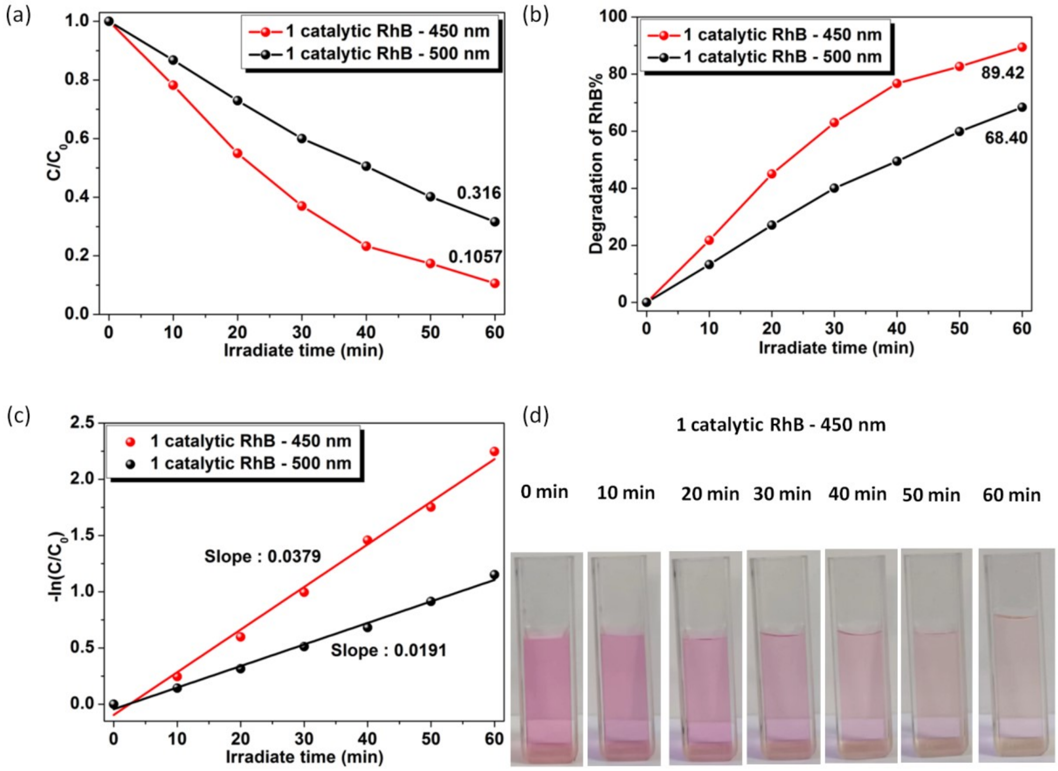

Figure S11. Photocatalytic degradation of RhB by photocatalyst **1** in neutral aqueous solution. (a) Decomposition curves, (b) percentage degradation, (c) corresponding apparent rate constants and (d) state after photocatalytic degradation for RhB. Reaction conditions: visible light (λ = 450 and 500 nm) at room temperature; [RhB] = 20 mg/L; Photocatalyst 10 mg.

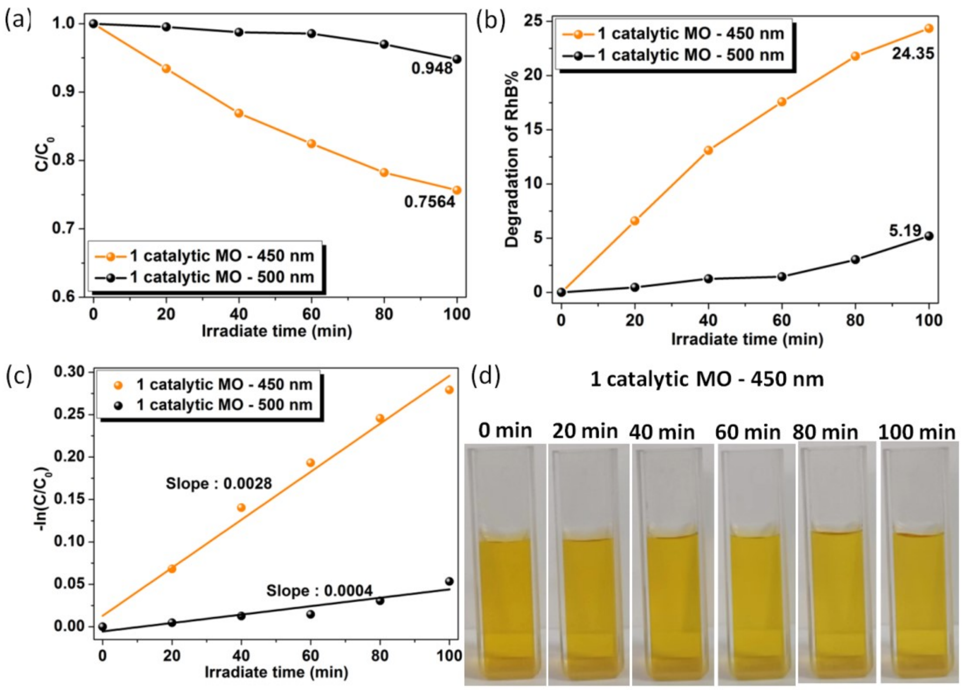

Figure S12. Photocatalytic degradation of MO by photocatalyst **1** in neutral aqueous solution. (a) Decomposition curves, (b) percentage degradation, (c) corresponding apparent rate constants and (d) state after photocatalytic degradation for MO. Reaction conditions: visible light (λ = 450 and 500 nm) at room temperature; [MO] = 20 mg/L; Photocatalyst 10 mg.

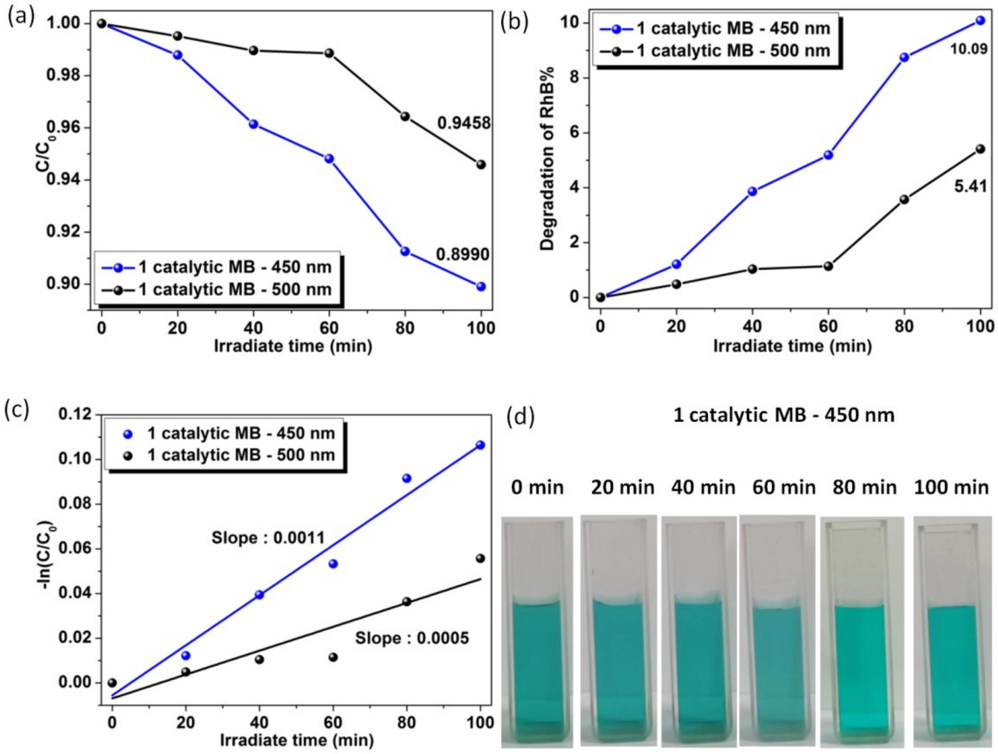

Figure S13. Photocatalytic degradation of MB by photocatalyst **1** in neutral aqueous solution. (a) Decomposition curves, (b) percentage degradation, (c) corresponding apparent rate constants and (d) state after photocatalytic degradation for MB. Reaction conditions: visible light (λ = 450 and 500 nm) at room temperature; [MB] = 10 mg/L; Photocatalyst 10 mg.

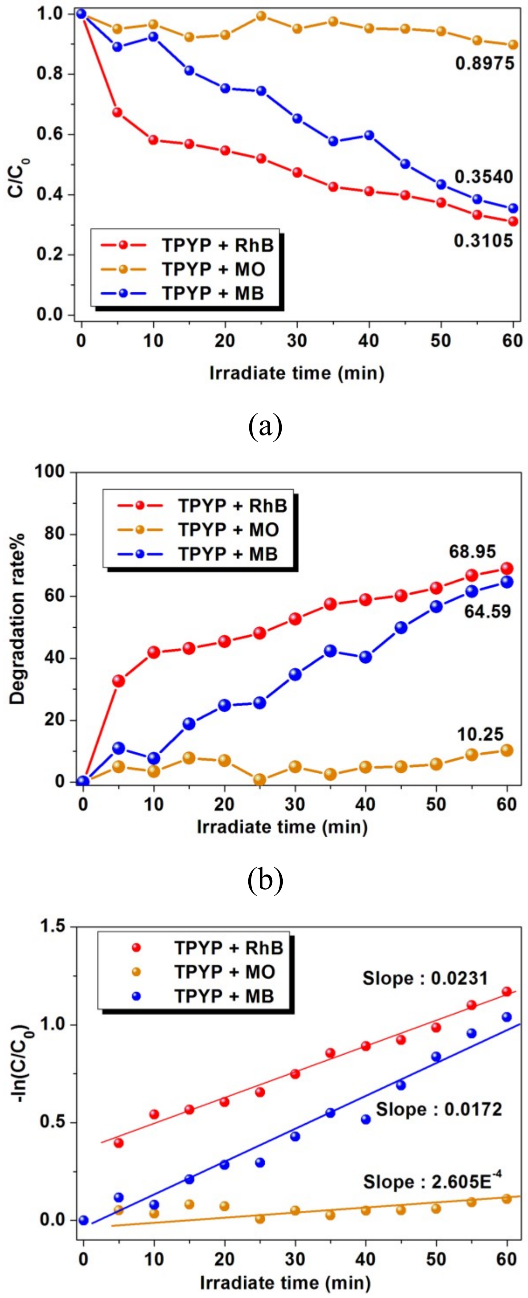

(a)

(b)

(c)

Figure S14. Photocatalytic degradation of dyes by TPyP in neutral aqueous solution. (a) Decomposition curves, (b) percentage degradation, and (c) corresponding apparent rate constants for the photocatalytic degradation of RhB, MO and MB. Reaction conditions: visible light (λ > 420 nm) at room temperature; [RhB] = 20 mg/L; [MO] = 20 mg/L; [MB] = 10 mg/L; TPyP: 10 mg.

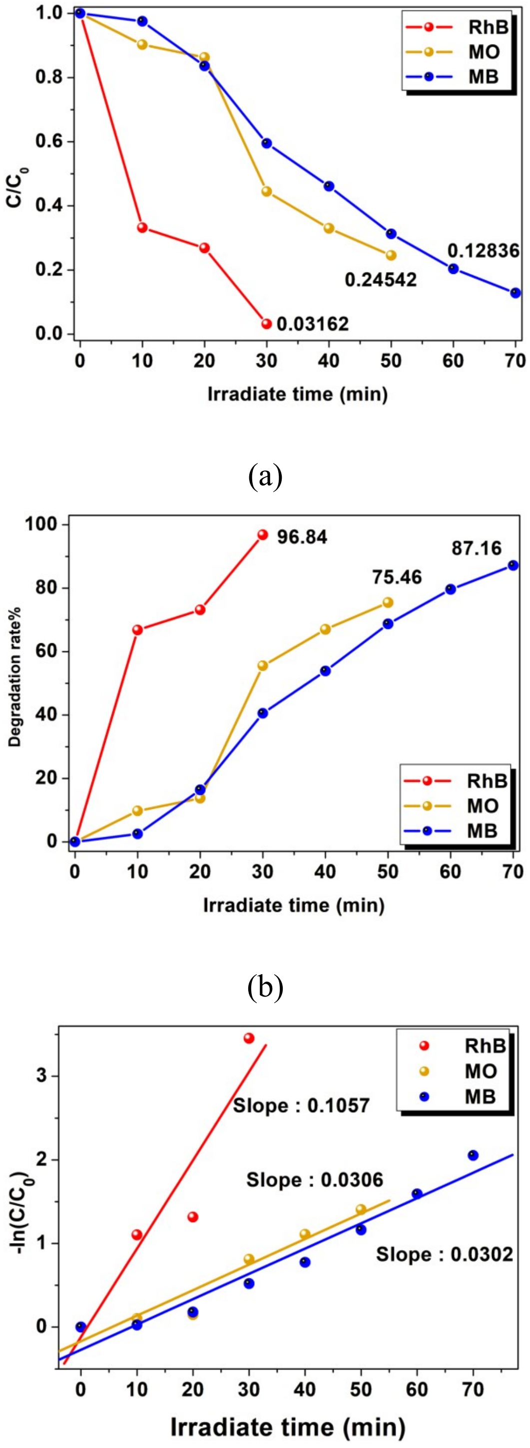

(a)

(b)

(c)

Figure S15. Photocatalytic degradation of a mixture of three dyes by **1** in neutral aqueous solution. (a) Decomposition curves, (b) percentage degradation, and (c) corresponding apparent rate constants Reaction conditions: visible light (λ > 420 nm) at room temperature; [RhB] = 20 mg/L; [MO] = 20 mg/L; [MB] = 10 mg/L; **1**: 10 mg.

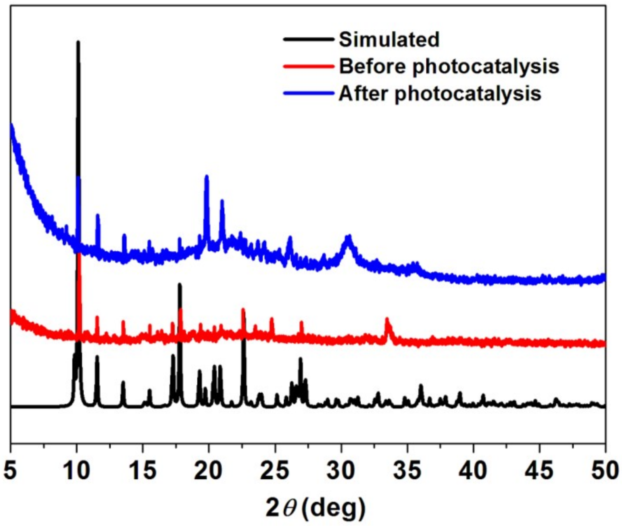

Figure S16. PXRD of **1** before and after photocatalysis.

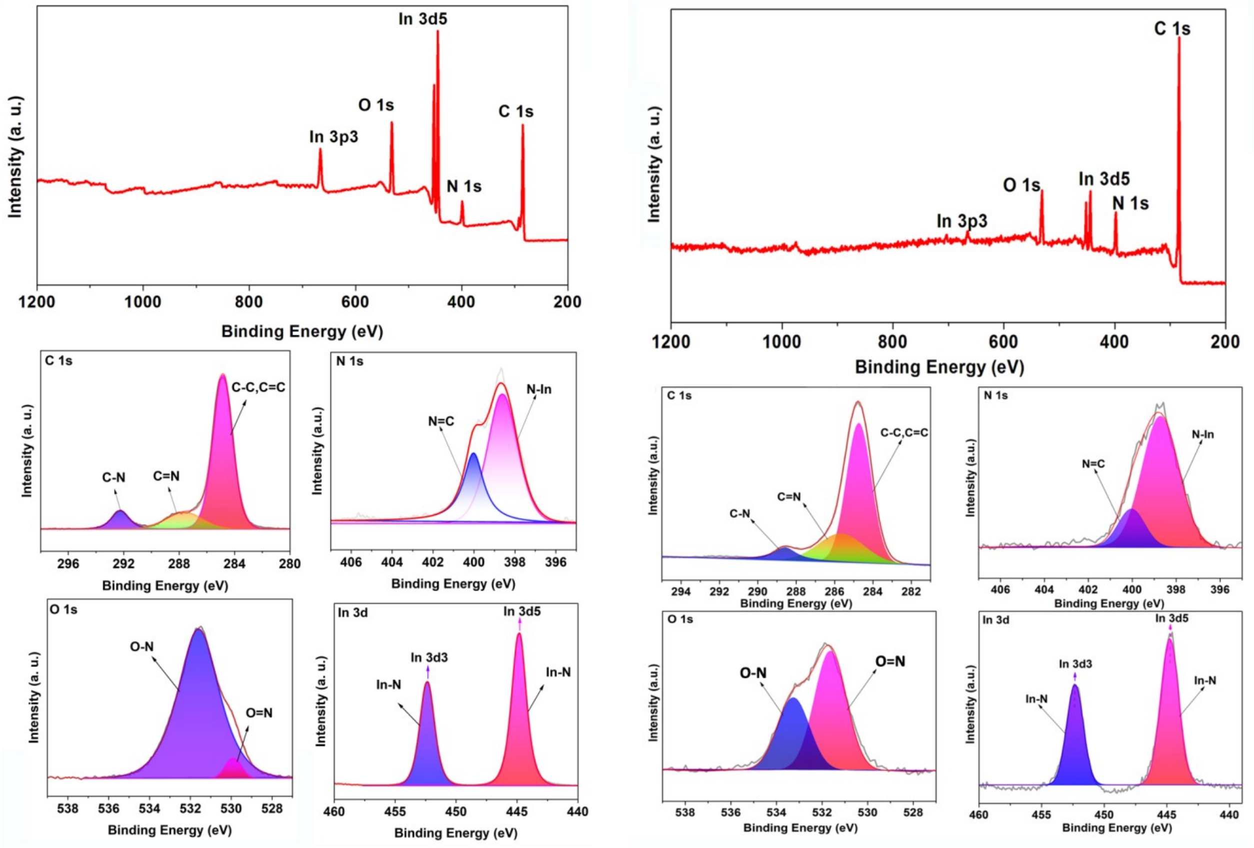

(a) (b)

Figure S17. The survey XPS spectrum and high-resolution XPS spectra of C 1s, N 1s, O 1s, In 3d for **1** before (a) and after (b) long-term photocatalytic experiments (λ > 420 nm).

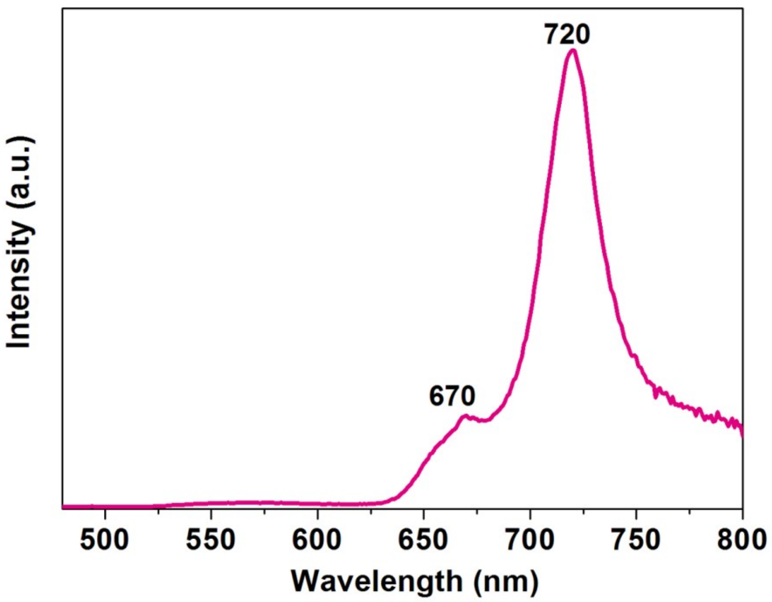

(a)

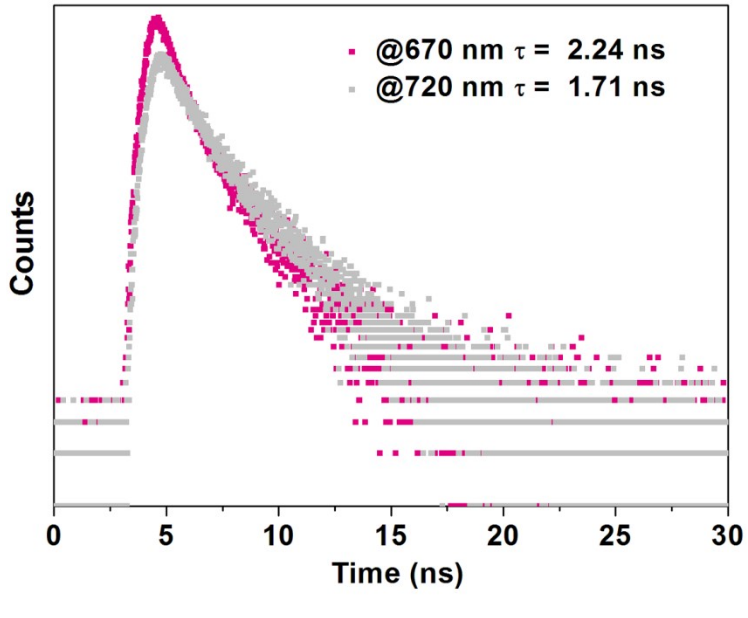

(b)

Figure S18. Fluorescence spectrum (c) and decay curves (d) of TPyP aqueous suspension (10 mg·L^{-1}).

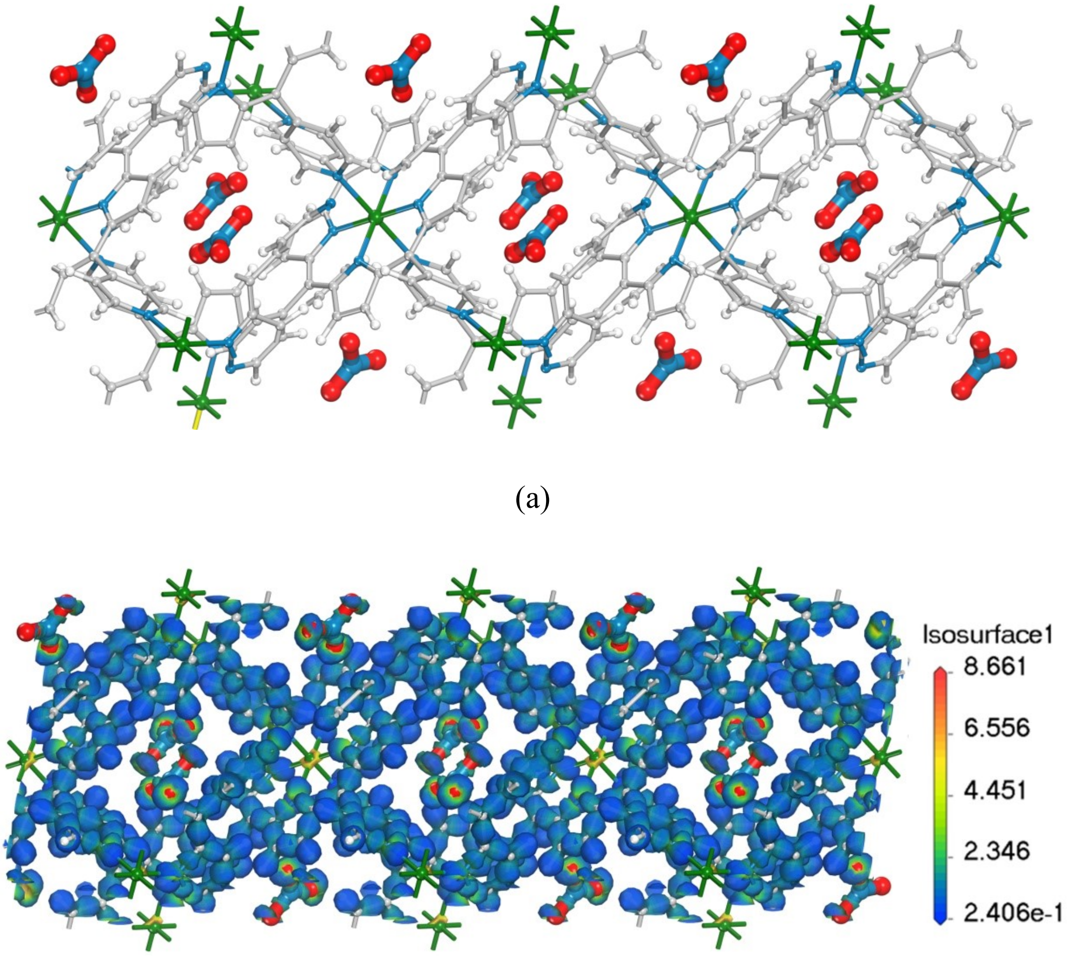

(a)

(b)

Figure S19. The DFT optimized 3D structure (a) and calculated charge density distribution (b) of **1**.

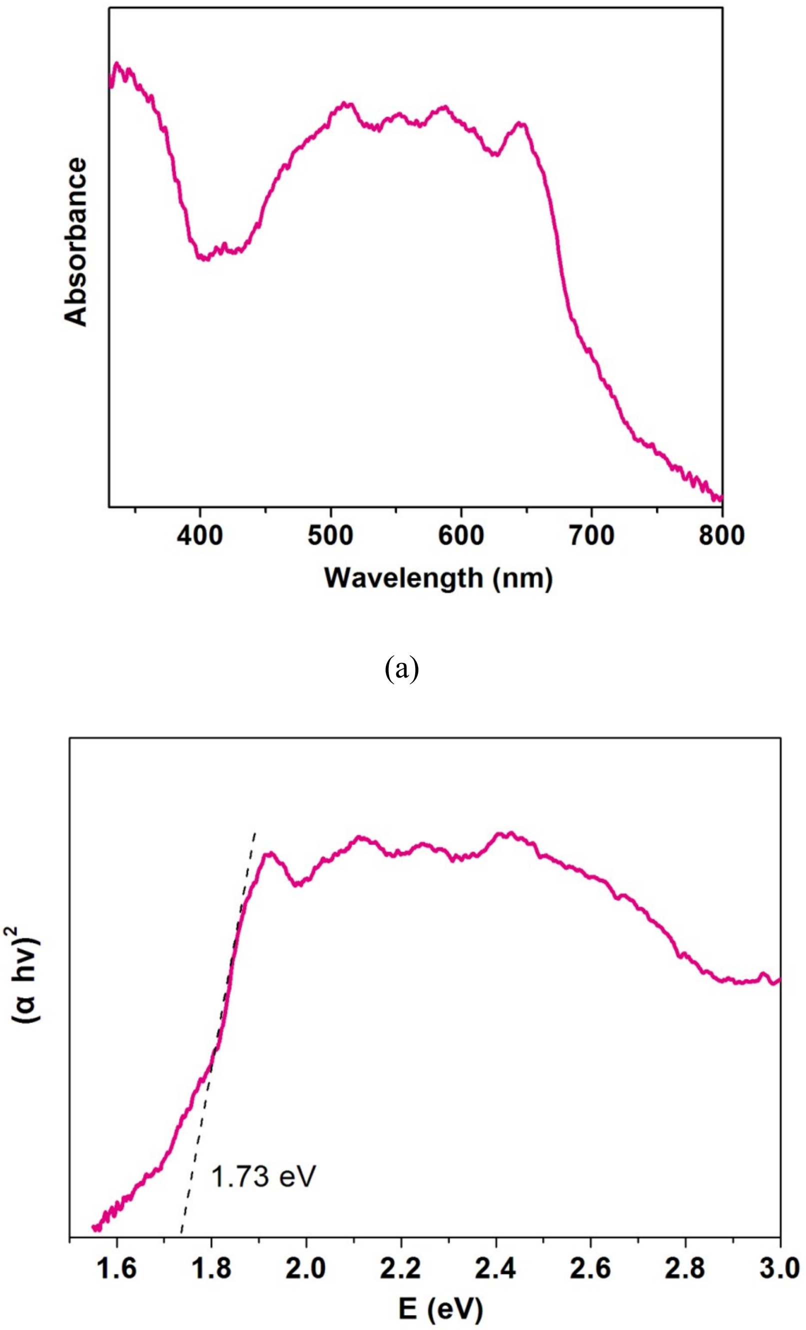

(a)

(b)

Figure S20. UV-vis spectrum (a) and Tauc plot (b) of complex **1** aqueous suspension (10 mg·L^{-1}).

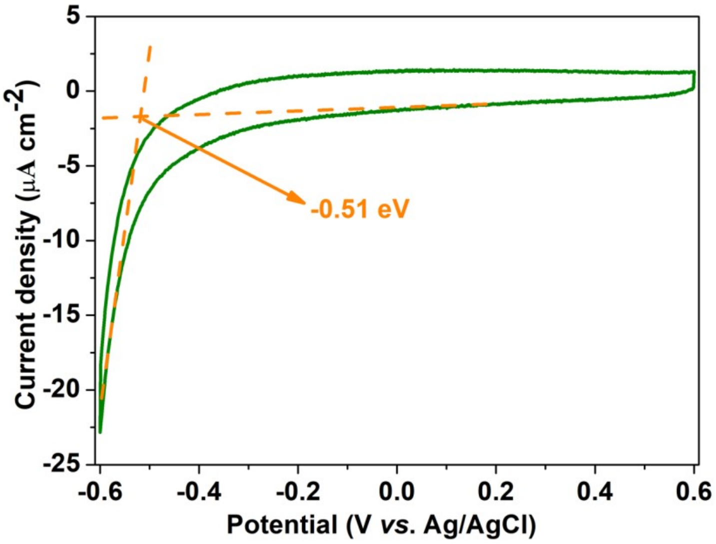

Figure S21. Cyclic voltammetric curve of complex **1**.

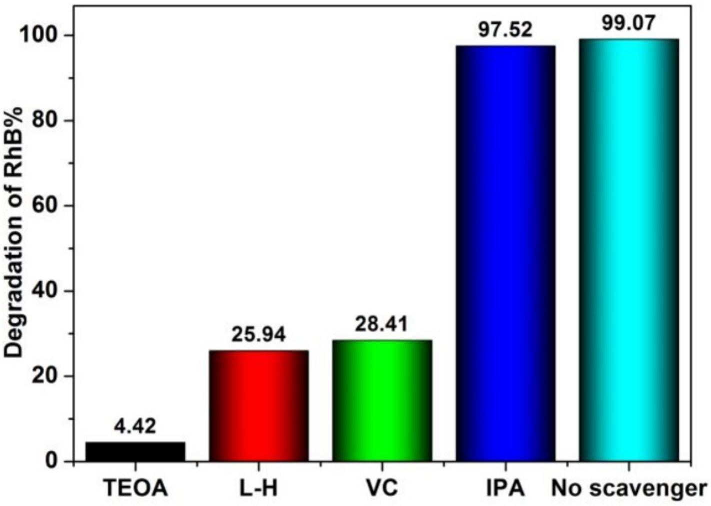

Figure S22. Bar chart of degradation rate changes of **1** after adding different scavengers. L-Histidine (L-H), Vitamin C (VC), Triethanolamine (TEOA) and propan-2-ol (IPA) was selected as trapping agent for the detection of singlet oxygen ($^1O_2$), superoxide radicals ($\cdot O_2^-$), hole (h^+) and hydroxyl radicals ($\cdot OH$), respectively.

C. Supporting Tables

Table S1. Crystallographic data for **1**.

Complex	**1**
Empirical formula	$C_{40}H_{24}InN_9O_3$
Formula weight	793.50
CCDC	2269364
Temperature/K	293(2)
Crystal system	monoclinic
Space group	$P2_1/n$
a/ Å	11.7675(3)
b/ Å	13.1064(4)
c/ Å	11.8764(4)
α/ °	90
β/ °	99.112(3)
γ/ °	90
V/Å^3	1808.58(10)
Z	2
D (g cm^{-3})	1.457
μ (mm^{-1})	0.705
R_{int}	0.0245
Goof	1.123
R_1 ($I>2\sigma(I)$)^a	0.0390
wR_2 ($I>2\sigma(I)$)^b	0.1060

$^aR_1 = \Sigma||F_o| - |F_c||/\Sigma|F_o|$, $^bwR_2 = [\Sigma w(F_o^2 - F_c^2)^2/\Sigma w(F_o^2)^2]^{1/2}$

Table S2. Selected bond distances /Å and bond angles /° for **1**.

In1-N2^{1}	2.373(3)	In1-N2^{2}	2.373(3)
In1-N3^{3}	2.128(3)	In1-N3	2.128(3)
In1-N4	2.109(3)	In1-N4^{3}	2.109(3)
N2^{1}-In1-N2^{2}	180.00(11)	N3-In1-N2^{2}	93.80(11)
N3-In1-N2^{1}	86.20(11)	N3^{3}-In1-N2^{2}	86.20(11)
N3^{3}-In1-N2^{1}	93.80(11)	N3-In1-N3^{3}	180.0
N4^{3}-In1-N2^{2}	90.29(11)	N4^{3}-In1-N2^{1}	89.71(11)
N4-In1-N2^{1}	90.29(11)	N4-In1-N2^{2}	89.71(11)
N4-In1-N3	90.15(11)	N4^{3}-In1-N3	89.85(11)
N4-In1-N3^{3}	89.85(11)	N4^{3}-In1-N3^{3}	90.15(11)
N4-In1-N4^{3}	180.0		

Symmetry operations: ^{1}1/2 - X, -1/2 + Y, 1/2 - Z; ^{2}1/2 + X, 3/2 - Y, 1/2 + Z; ^{3}1 - X, 1 - Y, 1 - Z.